



Capacitive charging rate dependence of heat from porous carbon in aqueous salt solution

Joren E. Vos, Ben H. Erne^{*}

Van 't Hoff Laboratory for Physical and Colloid Chemistry, Debye Institute for Nanomaterials Science, Utrecht University, Padualaan 8, 3584 CH Utrecht, The Netherlands

ARTICLE INFO

Keywords:

Porous electrodes
Electrical double layer
Supercapacitors
Capacitive deionization
Reversible heat

ABSTRACT

Porous capacitive electrodes are applied in supercapacitors and capacitive deionization of aqueous salt solutions. In both cases, electric charge and ions are stored in the electrical double layer at the surface of the pores. Recently, we revealed that the equilibrium potential energy of the ions in the pores can be obtained from isothermal calorimetric measurements. On that basis, we now introduce a model for the time-dependent heat production at any charging or discharging rate. The model centers on a mathematical expression for the time-dependent internal energy of the double layer, which depends only on constant system parameters and the time-dependent electric potential drop across the double layer. Semiquantitative agreement is found with experiments on a porous carbon electrode in aqueous salt solution. The theory applies both in the case of abrupt application of a potential to the electrode, generating a maximum amount of Joule heat, and in cases where the potential is applied more slowly, even when charging becomes so slow that heat production is essentially reversible. These results not only provide fundamental insight into the electrical double layer of porous capacitive electrodes, but they are also a new way to describe and to predict the time-dependent generation of heat from such electrodes.

1. Introduction

Whereas the main function of electrodes is to enable electrochemical conversions or to store electric charge or ions, electrodes also produce heat. In batteries and supercapacitors, most of the heat is Joule heat, generated by the flow of current through resistive parts of the system. The rate of Joule heat production scales with the current squared (I^2), which is why it is always exothermic and becomes larger as the device is (dis)charged at higher rate [1–4]. Excessive heat can be damaging to batteries [5,6] and supercapacitors [7,8], and it may even cause safety hazards [9,10]. In academic research, the (dis)charging rate of electrical energy storage devices can be decreased drastically, so that Joule heat production is suppressed and reversible heat—produced at a rate that scales linearly with the current (I)—becomes dominating [11,12]. A key characteristic of reversible heat is that it has a different sign depending on the direction of the electric current. Moreover, measurements of the reversible heat give specific information on electrode processes. In the case of batteries, the reversible heat corresponds to $T\Delta S$, where T is the absolute temperature and ΔS is the entropy change, which can also be obtained from the temperature-dependence of the open circuit potential [12–17]. In the case of porous capacitive electrodes, the reversible heat of (dis)charging the capacitor

informs on changes in the state of the electrical double layer inside the pores. In the present work, we focus on heat production by capacitive porous electrodes and its dependence on the (dis)charging rate.

Capacitive electrodes are usually based on microporous carbon and they have a great specific surface area, typically more than 1000 m² per gram of dry material. Such electrodes are used in the desalination of water via capacitive deionization [18–20] and the storage of electrical energy in supercapacitors [21–23]. Compared to nonporous electrodes, the (dis)charging of porous electrodes is relatively slow, limited by ionic transport through the porous network. Most transport occurs via mesopores (2–50 nm in width), whereas most storage of charge and ions occurs at the surface of micropores (<2 nm in width) [24–26]. The electrical double layer extends throughout the porous network, rendering interfacial heat effects sufficiently strong that they can be measured using sensors that detect temperature [3,27] or heat flux [11,28].

Reversible heat production by porous capacitive electrodes was first detected via temperature measurements on insulated supercapacitors. On top of an overall temperature rise, due to Joule heat, a reversible effect was observed, an increase in temperature during charging and a decrease in temperature during discharging. Schiffer et al. [3] attributed the reversible heat to the decrease in entropy

^{*} Corresponding author.

E-mail address: b.h.erne@uu.nl (B.H. Erne).

<https://doi.org/10.1016/j.electacta.2023.141957>

Received 21 October 2022; Received in revised form 24 January 2023; Accepted 25 January 2023

Available online 30 January 2023

0013-4686/© 2023 The Author(s). Published by Elsevier Ltd. This is an open access article under the CC BY license (<http://creativecommons.org/licenses/by/4.0/>).

when ions are confined into the electrical double layer during charging and the increase in entropy when the ions are released into bulk solution during discharging. Alternatively, Dandeville et al. [11] suggested that the reversible heat might be due to the adsorption energy of ions at the carbon surface. D'Entremont and Pilon [29,30] developed an elaborate physical model for the time-dependent thermal effects of (dis)charging a planar electrical double layer capacitor, using the Poisson–Nernst–Planck equations to describe electric potential gradients and ion transport, taking into account the finite size of the ions. In their model, energy conservation imposes the generation of heat when the ions experience gradients in their electrical potential energy and chemical potential, due to diffusion gradients, concentration-dependent steric repulsion, and electrical ion–ion interactions. This model also accounted for measured reversible and irreversible heat effects, and it was adapted to predict the temperature evolution in commercial supercapacitor devices during galvanostatic cycling [31]. Janssen and Van Roij [32] demonstrated that in the limit of slow charging, the kinetic approach of D'Entremont and Pilon agreed with equilibrium thermodynamics [33]. The same authors [32] and Porada et al. [34] noted that the cooling of the electrical double layer, mostly observed during discharging, can also be viewed as the result of ionic current being locally driven in direction opposite to the electric field at the solid–liquid interface.

The development of dedicated isothermal calorimeters led to new experimental and theoretical studies of heat production in a constant temperature environment. Munteshari et al. [28] built a calorimeter that used separate heat flux sensors for the two electrodes in a two-electrode cell. For carbon electrodes in aqueous and nonaqueous solutions, they found differences in heat production at positive and negative potentials. Janssen et al. [27] experimentally found that the reversible heat produced by a cell with two porous carbon electrodes in aqueous NaCl solution was approximately independent of salt concentration, from 1 to 1000 mM, and they identified the reversible heat as the entropic contribution to the grand potential energy cost of double layer formation. Glatzel et al. [35] used classical density functional theory and molecular dynamics simulations to test microscopic models of the double layer on the latter experimental results [27], describing ions as charged hard spheres in a homogeneous dielectric background (restricted primitive model). They found an important effect of ionic steric interaction with the carbon wall, corresponding to the presence of a Stern layer, and they also made predictions for the effects of ionic size, concentration, and valency on the reversible heat. This model was recently extended [36] to predict the impact of asymmetry in the sizes of the ions, distinguishing between the size of hydrated ions involved in ion–ion interactions and the size of the ions without hydration shell, setting the closest distance of approach of the ions to the carbon surface, at the cost of partial loss of the hydration shell. This model enabled the description of unequal heat production at positive and negative potentials, and it foresaw the possibility that the reversible heat produced during charging does not necessarily have to be exothermic.

In our own recent experimental work [37], we measured the isothermal heat of double layer formation in microporous carbon electrodes submerged in aqueous solutions of different types of ions, using a three-electrode configuration to perform the measurements as a function of electrode potential [38]. We proposed an analytical expression for the potential-dependent internal energy of the double layer, making it possible to calculate heat effects by subtracting the electrical work performed on the electrode from the change in internal energy. In that framework, reversible heat is produced when the internal energy not only consists of the electric field energy of the double layer capacitor but also includes other contributions, such as the attraction of ions to the electrode surface and the electrical energy of the ions inside the pores. However, in the experiments, electrode potentials were applied abruptly, and the reversible heat was calculated from the difference between the heats of charging and discharging, processes that were

carried out far from equilibrium. It was assumed that the Joule heat was precisely the same during charging and discharging, but earlier evidence in support of this assumption was not necessarily conclusive [27]. Moreover, no attempt was made to slow down the rate of (dis)charging, to diminish the Joule heat, so that the reversible heat might be determined directly as the main contribution to the measured heat.

In the present work, our model that describes the heat generated after abrupt application of an external potential to the electrode [37] is extended to describe the time-dependent heat generation at any (dis)charging rate. To compare the theory to the measurements, no fitting is required, except for an initial determination of constant system parameters from experiments in which the applied potential is set abruptly. In the Experimental section, our method to measure the heat of electrical double layer formation of porous capacitive electrodes is summarized. Our model is presented in the Theory section, and in the Results and Discussion section, results of the measurements are presented and compared one-to-one to predictions of the model.

2. Experimental

Experiments were conducted using the glass electrochemical cell described in Ref. [38]. The setup consisted of three electrodes: a microporous carbon working electrode (WE), an Ag/AgCl/saturated KCl reference electrode (RE, Radiometer REF201), and a counter electrode (CE). A PARSTAT PMC-1000 potentiostat was used to control the potential of the WE with respect to the RE and to measure the resulting current that flowed between WE and CE. The WE and CE were made of porous carbon disks, of the same material as used in Refs. [27,37,39]. As reported in Ref. [37], the disks had a diameter of 21 mm, a thickness of ~ 0.25 mm, a mass of 63 mg, a specific surface area of $1400 \text{ m}^2/\text{g}$ (88 m^2 per electrode), a porosity of 60%, and an average pore width of ~ 0.9 nm.

The heat generated at the WE was measured using a heat flux sensor (HFS, gSKIN[®] XP 26 9C, greenTEG AG, Switzerland). The resulting voltage was measured using a Keithley 2182A Nanovoltmeter. The glass cell was submerged in water in a box that was thermostated at 22°C by a Julabo F25 refrigerated/heating circulator. The cell was filled with a degassed solution of 1 M NaCl (Merck Emsure[®], for analysis), in water (Milli-Q, neutral pH).

Before polarization was started, the temperature of the system was left to stabilize for two days. During this time, the open circuit potential (V_{OCP}) was measured, stabilizing at a potential $V_{\text{OCP}} = 0.2 \text{ V}$ vs RE. Then, a potential of 0 V vs V_{OCP} was applied for an hour. Charging was initiated by changing the potential linearly in time until a final potential ΔV in the range from -0.5 to $+0.5 \text{ V}$ vs V_{OCP} was reached in a time τ , which was varied between 0 and 2000 s. After 2 h, the applied potential was changed back to 0 V vs V_{OCP} , also linearly in a time τ , to discharge the system. Then, the applied potential of 0 V vs V_{OCP} was kept stable for 2 h to allow the absolute current to become minimal ($\leq 20 \mu\text{A}$). For each polarization rate, the charge–discharge cycle was measured at least twice, leading to practically the same results.

As will be discussed in Section 3.3, our general approach to calibrate the HFS was as described in Refs. [37,38]. In essence, the integral signal of the sensor for a full charge–discharge cycle was scaled to the net electrical work that had been performed on the system during the cycle. The same calibration constant that was determined to convert integral HFS signal in Vs into energy in J was also used to convert time-dependent heat signal in V into heat production rate in W.

3. Theory

In this section, theory is presented to describe how the gradual buildup of the applied potential affects the time-dependent electric current and heat production. The studied experimental system consisted of an electrical double layer capacitor in an isothermal environment. This

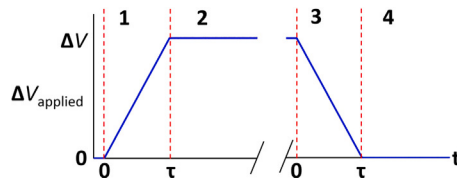


Fig. 1. Time dependence of the applied potential in the theory and the experiments. Charging starts with changing the potential from 0 V to ΔV in a time τ , followed by lengthy equilibration. Discharging starts by bringing the potential back to zero in a time τ , again followed by lengthy equilibration. Periods 1–4 are indicated.

system can be approximated by a resistor of resistance R connected in series to a capacitor of capacitance C . Although electrically, the capacitance describes the amount of stored charge as it would for any capacitor, its internal energy is different from that of a simple capacitor. The energy is also affected by interaction of the ions with the electrode surface and with the electric potential inside the pores, both of which affect the heat production. The general foundations of the model are presented in this section. The analytical formulas used to plot theoretical predictions in the Results and Discussion section are given in the [Appendix A](#), and details of the derivations are given as Supplementary Material.

3.1. Time-dependent applied potential

In our theory and experiments, the (dis)charging rate is controlled by changing the time taken to vary the applied potential linearly until a final value is reached. Four time periods are distinguished, see [Fig. 1](#). In period 1, the applied potential $\Delta V_{\text{applied}}$ is zero vs V_{OCP} at an initial time $t = 0$ s, and a time τ is taken to reach a final value ΔV :

$$\text{Period 1: } \Delta V_{\text{applied}}(t) = \frac{t}{\tau} \Delta V, \quad 0 \leq t \leq \tau. \quad (1)$$

In period 2, the applied potential is kept constant, and charging continues until current and heat production have become negligible:

$$\text{Period 2: } \Delta V_{\text{applied}}(t) = \Delta V, \quad t \geq \tau. \quad (2)$$

In period 3, discharging begins by resetting the time to $t = 0$ s. The applied potential now starts at a value ΔV , and this is brought back to zero in a time τ :

$$\text{Period 3: } \Delta V_{\text{applied}}(t) = \Delta V \left(1 - \frac{t}{\tau}\right), \quad 0 \leq t \leq \tau. \quad (3)$$

Finally, in period 4, the applied potential remains zero until current and heat production have become negligible:

$$\text{Period 4: } \Delta V_{\text{applied}}(t) = 0 \text{ V}, \quad t \geq \tau. \quad (4)$$

3.2. Time-dependent electric current

In each time period, the time-dependent current $I(t) = dQ(t)/dt$ can be approximated using Kirchoff's voltage law for a series RC circuit,

$$\frac{dQ(t)}{dt} = \frac{\Delta V_{\text{applied}}(t)}{R} - \frac{Q(t)}{RC}, \quad (5)$$

where the time-dependent charge $Q(t)$ is given by

$$Q(t) = Q_0 + \int_0^t I(t') dt' \quad (6)$$

and Q_0 is the charge present at the start of the period. The experimental resistance R can be calculated via Ohm's law from the peak current I_{peak} measured just after a potential step ΔV ($R = \Delta V / I_{\text{peak}}$). The experimental capacitance $C = \Delta Q / \Delta V$ can be calculated from the measured charge ΔQ .

3.3. First law of thermodynamics applied to capacitive electrodes

As discussed in [\[37\]](#), our experiments make it possible to calculate changes ΔU in the internal energy of the working electrode from the work w and the heat q , using the first law of thermodynamics:

$$\Delta U = w + q \quad (7)$$

In the system-centered sign convention, the internal energy can be increased ($\Delta U > 0$) by performing work on the system ($w > 0$) or by adding heat to the system ($q > 0$, endothermic effect). We assume that the only form of work that can occur is electrical work performed by the external electrical circuit. This can be calculated via

$$w(t) = \int_0^t \Delta V_{\text{applied}}(t') I(t') dt', \quad (8)$$

where $w(t)$ is the integral work at time t and $\Delta V_{\text{applied}}(t')$ is the applied potential at time t' . Pressure–volume work and chemical work are neglected. In our experiments, the heat effects are so small that differential temperature peaks are less than 0.1 °C, and the temperature is precisely the same before the start and after completion of (dis)charging [\[38\]](#). The system is therefore assumed to have a constant temperature.

Our approach to determine the amount of heat produced by the electrode from the signal of the heat flux sensor is as follows. The rate dq/dt of heat production is calculated from the voltage V_{HFS} of a heat flux sensor that is positioned against the electrode:

$$\frac{dq}{dt} = K V_{\text{HFS}} \quad (9)$$

The total amount of heat during charging or discharging is obtained by integrating dq/dt . The proportionality constant K is calculated from the integral HFS signal and the integral electrical work during a full cycle of charging plus discharging (ch+dis):

$$\oint_{\text{ch+dis}} I(t) \Delta V_{\text{applied}}(t) dt = -K \oint_{\text{ch+dis}} V_{\text{HFS}}(t) dt \quad (10)$$

The origin of this expression is that the energy change is zero for a full charge+discharge cycle ($\Delta U = 0$), because the system comes back to its initial state (same potential, charge, and temperature). Therefore, the total heat produced during a full cycle must be exactly opposite to the total electrical work performed on the electrode during the cycle. In [Ref. \[37\]](#), only the case of abrupt changes of the applied potential was considered, implying that the electrical work was $\Delta Q \Delta V$ during charging at potential ΔV and zero during discharging at 0 V.

3.4. Experimental potential dependence of the internal energy in equilibrium

For a simple parallel plate capacitor, the change in internal energy upon charging at a voltage ΔV is equal to the capacitor's final electrical energy:

$$\text{simple capacitor: } \Delta U = \frac{1}{2} C (\Delta V)^2 \quad (11)$$

Moreover, in the hypothetical case that charging is infinitely slow, in other words, carried out reversibly, all the electrical work performed on the capacitor would go toward changing the charge and the voltage. This implies that the reversible heat of a simple capacitor is zero ($q_{\text{rev}} = 0$). However, this is not what is found in calorimetric measurements on electrical double layer capacitors. Experimentally, their reversible heat is clearly nonzero.

In [Ref. \[37\]](#), we revealed that our measurements of the equilibrium internal energy of porous carbon electrodes in aqueous salt solutions could be described by the following expression:

$$\Delta U = \left(\frac{1}{2} - \frac{3}{2}f\right) C (\Delta V)^2 + C \Delta V \Delta V_{\text{att}}, \quad (12)$$

where $f > 0$ (dimensionless) and ΔV_{att} (in V) are fit constants. [Eq. \(12\)](#) indicates that the experimental internal energy consists of a term that

is quadratic in the applied potential, but smaller than expected for a simple capacitor [Eq. (11)], and a term that is linear in ΔV . In Ref. [37], we gave tentative physical explanations for the two terms. The linear term scales with the net ionic charge ($-C\Delta V$), and it was attributed to the adsorption energy of the ions, in line with the finding that this term was found to be negative. The quadratic term's difference compared to a simple capacitor was attributed to the average electrical potential energy of the ions inside the pores. It was assumed that the net ionic charge was added at constant electric potential $f\Delta V$ inside the porous network. Since, for large applied potentials, most of the net ionic charge is carried by counterions, adsorbed or not, the potential $f\Delta V$ is an average electric potential of the counterions at their positions inside the pores, for instance at a Stern layer distance from the carbon surface.

3.5. Time-dependent heat production

Eq. (12) was previously found to describe the internal energy of the electrical double layer in equilibrium [37]. In the present work, we propose that a similar expression can also be used to describe the heat's time dependence. We assume that at any instant, the internal energy of the electrical double layer is given by

$$\Delta U(t) = \left(\frac{1}{2} - \frac{3}{2}f\right) C(\Delta V_C(t))^2 + C\Delta V_C(t)\Delta V_{\text{att}}, \quad (13)$$

where $\Delta V_C(t) = Q(t)/C$ is the time-dependent potential drop across the electrical double layer capacitor. This excludes the potential drop across resistive elements of the electrical circuit, which is nonzero as long as equilibrium has not yet been attained. In the limit that $t/(RC)$ goes to infinity, $\Delta V_C(t)$ becomes ΔV and Eq. (13) reduces to Eq. (12). The rationale for Eq. (13) is that the potential drop across the capacitor at time t is what determines the field energy of the double layer as well as the net ionic charge at that instant. It is assumed that the adsorption enthalpy and the electrical potential energy of the ions scale with the ionic charge in the same way as under equilibrium conditions [Eq. (12)]. In the framework of the present work, where the gradual buildup of the electrical double layer is examined, one could also have chosen to define the average potential of the ions as a fraction f^* of $\Delta V_C(t)$. Following the derivation in Ref. [37], the electrical potential energy of the ions would then be given by the integral of $-CVf^*dV$ for V going from 0 to $\Delta V_C(t)$, giving a contribution of $-(1/2)f^*C(\Delta V_C(t))^2$ to the ionic potential energy and changing $-(3/2)f$ into $-f^*$ in Eq. (13).

The integral heat having been produced at time t can now be obtained using the first law of thermodynamics:

$$q(t) = \Delta U(t) - w(t), \quad (14)$$

where $\Delta U(t)$ is given by Eq. (13) and $w(t)$ can be calculated via Eq. (8), using either the measured time-dependent current or the $I(t)$ function predicted by the RC circuit model. The heat production rate at time t is finally found by differentiating Eq. (14):

$$\frac{dq(t)}{dt} = \frac{d\Delta U(t)}{dt} - \frac{dw(t)}{dt}. \quad (15)$$

4. Results and discussion

4.1. Determination of system constants

To predict the time-dependent current and heat production via the model presented in the Theory section, four system constants need to be known: the resistance R , the capacitance C , and the parameters f and ΔV_{att} that feature in Eq. (13) for the internal energy.

A resistance R of $11.0 \pm 0.6 \Omega$ was calculated from the initial current upon abrupt application of a potential ΔV to the electrode, using Ohm's law. The capacitance C was $(5.50 \pm 0.03) \text{ F}$ at $+0.5 \text{ V}$, $(5.34 \pm 0.02) \text{ F}$ at $+0.3 \text{ V}$, $(6.45 \pm 0.04) \text{ F}$ at -0.3 V , and $(6.87 \pm 0.02) \text{ F}$ at -0.5 V . The values of R and C indicate that the RC time was $\sim 60 \text{ s}$ during anodic (dis)charging and $\sim 73 \text{ s}$ during cathodic (dis)charging. However, for

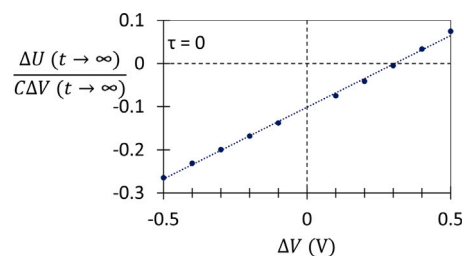


Fig. 2. Internal energy change per electrode charge measured upon abrupt polarization, plotted versus the applied potential. As introduced in Ref. [37], such a plot gives the system parameters that describe the potential energy of the ions in the pores. Using Eq. (13) with $\Delta V_C(t) = \Delta V$, $\Delta V_{\text{att}} = (-0.101 \pm 0.005) \text{ V}$ and $[-\frac{1}{2} - \frac{3}{2}f] = 0.333 \pm 0.002$ were obtained, corresponding to $f = 0.112$.

each individual charge–discharge cycle, the RC time was practically the same upon charging and discharging.

To calculate electrode heat from heat flux sensor voltage, first a calibration was carried out as discussed in Section 3.3. For full charge–discharge cycles, the net electrical energy input was plotted against the integral voltage of the heat flux sensor, according to Eq. (10). The calibration constant, corresponding to the slope of the plot, was independent of the finally reached applied potential and insensitive to the (dis)charging rate. It ranged from $(-368 \pm 5) \text{ J V}^{-1} \text{ s}^{-1}$ upon abrupt polarization to $(-439 \pm 40) \text{ J V}^{-1} \text{ s}^{-1}$ for a buildup time $\tau = 1000 \text{ s}$. However, the slower the changes in applied potential, the longer the signals had to be integrated and the larger the error was due to noise and background values of the current and HFS signal. These errors were the smallest for the calibration constant obtained from abrupt polarization experiments, which was used to analyze all the heat data.

The parameters f and ΔV_{att} in Eq. (12) were determined by measuring changes in the internal energy ΔU after prolonged charging at applied potential ΔV , see Fig. 2. As in Ref. [37], the experimental changes in internal energy were determined using the first law of thermodynamics [Eq. (7)], from the integral measured heat and the integral electrical work performed on the system, calculated via Eq. (8) from the time-dependent current at constant applied potential.

4.2. Abrupt polarization ($\tau = 0 \text{ s}$)

Fig. 3 shows theoretical predictions and experimental results for the case of $\tau = 0 \text{ s}$. A potential of $\Delta V = 0.5 \text{ V}$ was applied abruptly to the electrode, leading to a sudden current peak, which then exponentially decayed to zero. Except for the sign of the current, the current transients were practically the same during charging and discharging. The theoretical current values largely match the experiments, although in the measured curves, the time constant of exponential decay appears to increase gradually. This indicates that our theoretical description of the system in terms of a single RC time is oversimplified. The current transients would be better described by a distribution of relaxation times, partly due to spatial gradients of the electric potential experienced by the ions inside the pores [40] and polydispersity of the pore dimensions in conjunction with pore-size-dependent ionic mobilities [23,41–44].

Heat production was exothermic (negative) both during charging and discharging. However, the heat of discharging was much smaller than the heat of charging. This was because the reversible heat was negative during charging and positive during discharging. The theoretical heat curves largely reproduce the measurements, although the experimental heat curves were not as sharply peaked. Heat produced by the electrode had to flow through a glass barrier before reaching the heat flux sensor [38], resulting in a slight delay between heat production and detection.

Results as in Fig. 3 but for other values of ΔV are provided in the Supporting Materials.

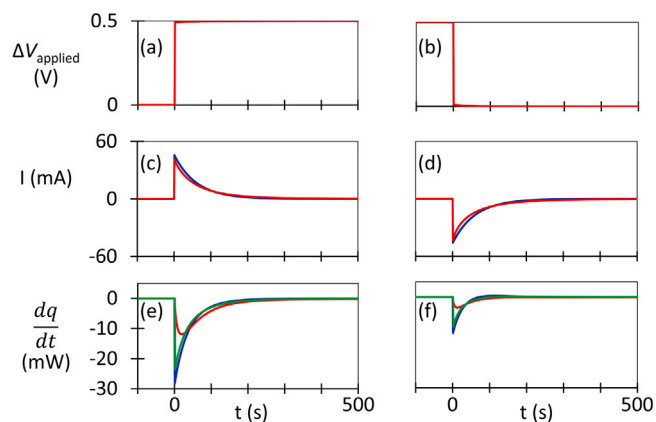


Fig. 3. Theoretical (blue and green) and experimental (red) time-dependence of electric current and heat production rate in the case of abrupt changes of the potential applied to a capacitive porous carbon electrode in 1 M NaCl ($\tau=0$ s, charging potential $\Delta V=0.5$ V). Time dependence of (a, b) the applied potential, (c, d) the electric current, and (e, f) the heat production rate (an instrumental offset of 0.86 mW was subtracted). The theoretical time-dependent current was calculated using (c, d) Eq. (A.3) and the heat production rate was calculated using (e) Eq. (A.6) (charging) and (f) Eq. (A.9) (discharging). The values for f and ΔV_{att} were those found in Fig. 2. The green curves in (e, f) were calculated using the measured $I(t)$ values and Eqs. (8), (13), and (15), rather than using the RC circuit-based model.

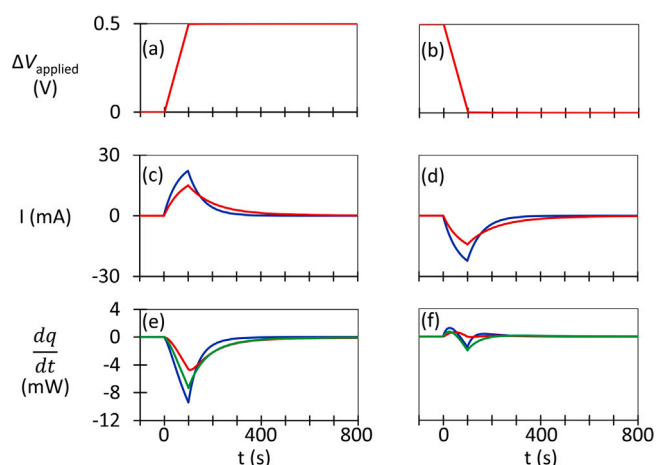


Fig. 4. As in Fig. 3, but now for gradual change of the applied potential, with $\tau=100$ s ($\Delta V=0.5$ V, same f and ΔV_{att} as in Fig. 2). In (e) and (f), an instrumental offset of 0.74 mW was subtracted. The theoretical time-dependent curves were calculated using (c, d) Eqs. (A.1) and (A.2) for the current, (e) Eqs. (A.4) and (A.5) for the heat production rate during charging, and (f) Eqs. (A.7) and (A.8) for the heat production rate during discharging.

4.3. Intermediate charging rate ($\tau=100$ s)

Fig. 4 shows measurements and theory for the case that a time $\tau=100$ s was taken to apply $\Delta V=0.5$ V. Note that 100 s has the same order of magnitude as the RC time. In theory and experiment, the current became larger while the applied potential changed, both during charging and discharging. At $t=100$ s, the applied potential stopped changing, and the current started to decay exponentially toward zero, with a characteristic time constant equal to RC. The current did not increase as rapidly in experiment as in theory, which probably is again because the description in terms of a single RC time is oversimplified.

The time-dependent heat production was now even more different between charging and discharging than in the case of abrupt polarization. During charging, the heat production rate mirrored the current, first increasing more or less linearly and then decaying exponentially. The measured heat production was lower than in theory, probably

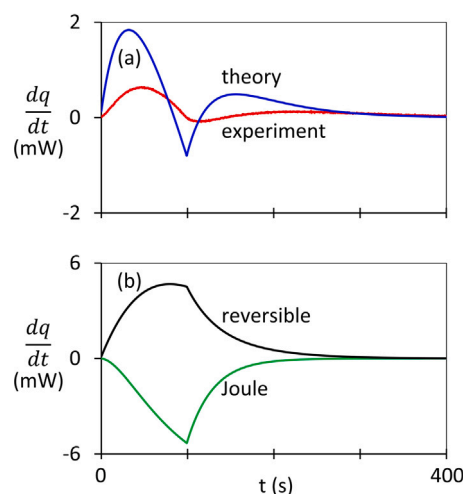


Fig. 5. (a) Experimental (red) and theoretical (blue) total heat production rate for $\tau=100$ s and $\Delta V=0.5$ V, as in Fig. 4(f). (b) Separate contributions of reversible heat (black) and irreversible heat (green). The curve for the irreversible heat production rate was calculated by filling in $f=0$ and $\Delta V_{\text{att}}=0$ V into Eqs. (A.7) and (A.8). The curve for the reversible heat production rate was found by subtracting the irreversible contribution from the total heat production rate, calculated using the same equations but with the values of f and ΔV_{att} found in Fig. 2.

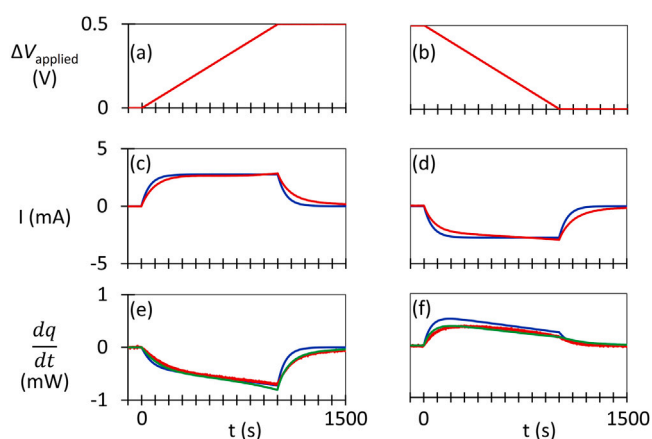


Fig. 6. As in Fig. 3, but now for gradual change of the applied potential, with $\tau=1000$ s ($\Delta V=0.5$ V, same f and ΔV_{att} as in Fig. 2). In (e) and (f), an instrumental offset of 0.73 mW was subtracted. The theoretical time-dependent curves were calculated in the same way as in Fig. 4.

because the lower than theoretical electric currents led to lower than theoretical production of Joule heat. During discharging, theory predicted that the produced heat would first be positive (endothermic), indicating that the reversible heat was larger than the Joule heat, but that before $t=100$ s, heat production would become negative, indicating that Joule heat had become dominating. After $t=100$ s, heat production would again decay to zero. Fig. 5 shows a close-up of Fig. 4(f) as well as the predicted time-dependent contributions of reversible and irreversible heat. These two contributions are relatively large, but they partly cancel each other out. In experiment, the predicted effects are smoothed out by the delay between heat production and detection.

Results as in Fig. 4 for $\tau=100$ s, but for other values of ΔV , are provided in the Supporting Materials.

4.4. Nearly reversible charging ($\tau=1000$ s)

Fig. 6 shows measurements and theory for the case that a time $\tau=1000$ s was taken to apply $\Delta V=0.5$ V ($\tau \sim 15RC$). After a time of

about $2RC$, the current stayed approximately constant until $t = 1000$ s, after which it exponentially decayed toward zero. The theoretical current transients match the measurements fairly well. From Eq. (A.1), it can be deduced that in the plateau, the current was approximately equal to $C\Delta V/\tau$.

The heat production transients for $\tau = 1000$ s started to approach a fully reversible situation. Irreversible heat production was so small that during discharging, the heat production remained positive from beginning to end. Moreover, the total heat production during charging was now of similar magnitude but opposite in sign to that during discharging. After $t = 1000$ s, the heat production again exponentially decayed toward zero. Note that in Fig. 6, the green curves (calculated from the measured $I(t)$ via Eqs. (8), (13), and (15)) give a closer fit to the data (in red) than the equations that describe the current using the RC circuit-based model.

Results as in Fig. 6 for $\tau = 1000$ s, but for other values of ΔV , are provided in the Supporting Materials.

4.5. Total heat of (dis)charging as a function of polarization rate

In Fig. 7, the total heat of charging (q_{ch}) and the total heat of discharging (q_{dis}) are plotted against the applied potential buildup time τ at four different charging potentials. At all potentials, both the charging and discharging heats became more positive with increasing polarization time τ , and the total heat $q_{ch} + q_{dis}$ of a full charge-discharge cycle evolved toward zero. This indicates that q_{ch} and q_{dis} progressed toward the same absolute value, but with opposite sign. In other words, the reversible heat became dominating. However, even at the slowest charging rate ($\tau = 2000$ s), the heat was not yet fully reversible.

The charging and discharging heats depended on the charging potential. At $\Delta V = 0.5$ V and $\Delta V = 0.3$ V, the charging heat was more negative than the discharging heat, but at $\Delta V = -0.3$ V, it was the other way around. This indicates that the reversible heat of charging was negative at $\Delta V = 0.5$ V and $\Delta V = 0.3$ V but positive at $\Delta V = -0.3$ V. At $\Delta V = -0.5$ V, the heats of charging and discharging were almost the same, indicating that the reversible heat was close to zero. Although the theoretical curves do not describe the measurements quantitatively, the sign reversal of the reversible heat is reproduced, as well as the trends in the magnitude of the reversible and Joule heats.

In the measured and calculated curves in Fig. 7, the difference between the heats of charging and discharging is independent of the charging rate. In Refs. [27,37], the difference between q_{ch} and q_{dis} upon abrupt polarization was equated to twice the reversible heat, assuming that the Joule heat was identical upon charging and discharging. This assumption is supported by the model in the present work. The same expression for the absolute reversible heat $|q_{rev}|$ is found in the limit of infinitely slow charging and discharging, Eq. (A.14). Moreover, since the RC time was the same for charging and discharging, the total Joule heat q_{irr} is found to be the same during charging and discharging, regardless of the time τ that is taken to apply the final potential ΔV to the electrode (given by Eq. (A.16) for $\tau = 0$ or Eq. (A.15) for $\tau > 0$). The combination of these theoretical results confirms that the difference between the heat of charging, $q_{ch} = q_{irr,ch} + q_{rev}$, and the heat of discharging, $q_{dis} = q_{irr,dis} - q_{rev}$, is indeed equal to $2q_{rev}$. This supports the validity of the earlier presented analysis of heats of double layer formation from measurements where the electric potential was applied abruptly [37]. This also has an important practical implication, since measurements in which the potential is applied abruptly are shorter and lead to stronger signals than if the charging would have to be extremely slow to obtain valid thermodynamic information about the electrical double layer.

In the future, more theoretical work will be welcome to explain the physical origins of the empirical expression for the internal energy of the double layer, Eq. (12). Theory by Glatzel et al. [35] already

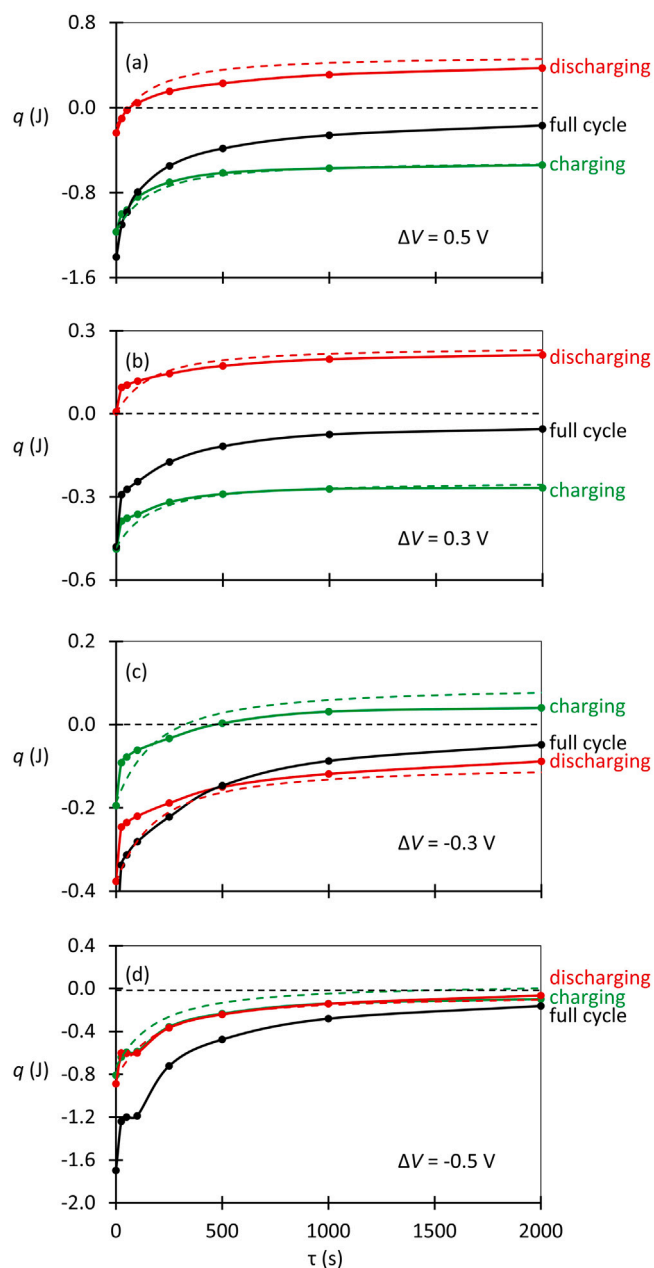


Fig. 7. Heats of charging and discharging versus time τ taken to apply or to remove potentials ΔV of (a) $+0.5$ V, (b) $+0.3$ V, (c) -0.3 V, and (d) -0.5 V. The total heats measured for full charge-discharge cycles are indicated as well. The dashed curves were calculated by filling in the values of f and ΔV_{att} found in Fig. 2 into Eqs. (A.10)–(A.13).

successfully predicted qualitative trends observed in our earlier experiments [37]: the larger the ions and the higher the salt concentration or ion valencies, the smaller the reversible heat scaled to the electrical work. Moreover, recent work by Pelagejcev et al. [36] was able to predict differences between reversible heat produced by single electrodes at positive and negative potentials. However, some aspects of these theories seem incompatible with experimental observations. These theories appear to require pore widths of no less than 10 nm to reproduce experimental values of the reversible heat scaled to the electrical work, while in experiments, most of the solid-electrolyte interface is found inside micropores (<2 nm). The experimental evidence for this is overwhelming, for instance capacitance measurements on carbon materials with monodisperse micropores (without larger pores) and the specific capacitance on the order of $6 \mu\text{Fcm}^{-2}$ found

for such materials [45,46] as well as for our electrodes (about 5 F per 88 m² electrode surface [37]), in relatively good agreement with the capacitance of flat, nonporous carbon electrodes in similar aqueous electrolyte solutions [47,48]. Moreover, the theories in Refs. [35,36] assume that water inside the pores has the dielectric constant of bulk water ($\epsilon_r \sim 80$), while in experiments, much lower values are generally assumed [39] and the dielectric constant of water has even been measured directly between atomically flat electrodes separated by merely 1 nm ($\epsilon_r \sim 2$) [49]. It is noted that a lower dielectric constant of water in the double layer implies that double layer overlap is less than if the dielectric constant would be that of bulk water. At low ionic strengths, double layer overlap is the basis for theory that assumes a modified Donnan equilibrium between inside and outside of the porous network [39]. The theoretical assumption of pores that are much larger than in experiment implies that the active surface area is much lower. This leads to high theoretical packing densities of adsorbed counterions and strong steric repulsion effects between these ions, effects that play a key role in the predicted reversible heat. In theory, a possible alternative way to increase ionic surface packing densities might be to take into account an additional adsorption mechanism of the ions, as evidenced experimentally by the spontaneous absorption of neutral salt by porous carbon at open circuit potential [39].

As an outlook toward new experimental work, we now first aim to investigate the effects of electric charge from dissociated surface chemical groups on our thermodynamic measurements. In Ref. [37], we ascribed the linear contribution to the attraction of ions to the carbon surface. However, chemical surface charge may also be partly responsible for the linear potential-dependent term in our expression for the internal energy of the electrical double layer [Eq. (12)].

5. Conclusions

Time-dependent and integral heat production were measured for a capacitive porous carbon electrode in 1 M aqueous NaCl. Different charging rates were realized by changing the time taken to build up the applied potential linearly to its final value ΔV . The reversible and irreversible heat effects were accounted for by a model that assumes that the internal energy of the electrode at time t depends on the potential drop across the electrical double layer at that instant. The system-dependent parameters of the model are four constants: the resistance, the capacitance, and f and ΔV_{att} , which describe the potential energy of the ions in the pores. When the electrode is being (dis)charged, the time-dependent heat production corresponds to the difference between the rate at which the internal energy changes and the rate at which electrical work is performed on the electrode. The analytical formulas derived on this basis are in semiquantitative agreement with the measured heat signals, which supports our theoretical approach. In the future, this model might be expanded to take into account a distribution of RC time constants or a gradual increase in temperature of the system, as occurs during the relatively rapid current or voltage cycling of a supercapacitor. In that case, it will be necessary to consider that the electrode is not fully charged or discharged during each half cycle. In this way, the thermodynamic approach presented here not only gives insight into the electrical double layer of porous capacitive electrodes, but it may also provide new insight into the reversible contribution to the production of heat by supercapacitors.

CRedit authorship contribution statement

Joren E. Vos: Data analysis, Methodology, Software, Investigation, Writing – original draft, Writing – review & editing. **Ben H. Ern :** Conceptualization, Methodology, Software, Writing – original draft, Writing – review & editing, Funding acquisition.

Declaration of competing interest

The authors declare that they have no known competing financial interests or personal relationships that could have appeared to influence the work reported in this paper.

Data availability

Data will be made available on request.

Acknowledgments

Maarten Biesheuvel is thanked for the carbon electrode material, Bonny Kuipers for technical support, and Marieke Nauta for preliminary experiments. This publication is part of the project ‘Experimental Thermodynamics of Ion Confinement in Porous Electrodes’ with project number 712.018.001 of the research program ECHO financed by the Dutch Research Council (NWO).

Appendix A. Main formulas for time-dependent current and heat

Derivations of the following formulas for the time-dependent current and heat in time periods 1–4 (see Fig. 1) can be found in the Supplementary Materials.

A.1. Time-dependent charging current

Below are formulas for the time-dependent charging currents. For discharging, the formulas are the same except that the current is negative.

Period 1 ($\tau > 0$):

$$I_{\text{ch},1}(t) = \frac{C\Delta V}{\tau} \left[1 - \exp\left(-\frac{t}{RC}\right) \right]. \quad (\text{A.1})$$

Period 2 ($\tau > 0$):

$$I_{\text{ch},2}(t) = I_{\text{ch},1}(\tau) \exp\left[-\frac{t-\tau}{RC}\right]. \quad (\text{A.2})$$

Abrupt ($\tau = 0$):

$$\lim_{\tau \rightarrow 0} I_{\text{ch},2}(t) = \frac{\Delta V}{R} \exp\left[-\frac{t}{RC}\right]. \quad (\text{A.3})$$

A.2. Time-dependent heat production rate

For discharging, the formulas do not have precisely the same form as for charging, because of the different initial charge and potential.

Charging, period 1 ($\tau > 0$):

$$\begin{aligned} \frac{dq_{\text{ch},1}(t)}{dt} = & \frac{C(\Delta V)^2}{\tau^2} \left[-3ft + (2-6f)RC \exp\left(-\frac{t}{RC}\right) - [1-3f]RC \right. \\ & \left. + 3ft \exp\left(-\frac{t}{RC}\right) - [1-3f]RC \exp\left(-\frac{2t}{RC}\right) \right] \\ & + C\Delta V_{\text{att}} \frac{\Delta V}{\tau} \left[1 - \exp\left(-\frac{t}{RC}\right) \right]. \end{aligned} \quad (\text{A.4})$$

Charging, period 2 ($\tau > 0$):

$$\begin{aligned} \frac{dq_{\text{ch},2}(t)}{dt} = & \frac{C(\Delta V)^2}{\tau} \left\{ -3f \exp\left[-\frac{t-\tau}{RC}\right] - [1-3f] \frac{RC}{\tau} \exp\left[-2\frac{t-\tau}{RC}\right] \right. \\ & \left. + 2[1-3f] \frac{RC}{\tau} \exp\left[-\frac{2t-\tau}{RC}\right] + 3f \exp\left(-\frac{t}{RC}\right) \right. \\ & \left. - [1-3f] \frac{RC}{\tau} \exp\left[-\frac{2t}{RC}\right] \right\} \\ & + \frac{C\Delta V \Delta V_{\text{att}}}{\tau} \left\{ \exp\left[-\frac{t-\tau}{RC}\right] - \exp\left(-\frac{t}{RC}\right) \right\}. \end{aligned} \quad (\text{A.5})$$

Charging ($\tau = 0$):

$$\lim_{\tau \rightarrow 0} \frac{dq_{ch,2}(t)}{dt} = \frac{(\Delta V)^2}{R} \left[-3f \exp\left(-\frac{t}{RC}\right) - [1 - 3f] \exp\left(-\frac{2t}{RC}\right) \right] + \frac{\Delta V \Delta V_{att}}{R} \exp\left(-\frac{t}{RC}\right). \quad (A.6)$$

Discharging, period 3 ($\tau > 0$):

$$\frac{dq_{dis,3}(t)}{dt} = \frac{C(\Delta V)^2}{\tau^2} \left[3f\tau - 3ft + [1 - 3f]2RC \exp\left(-\frac{t}{RC}\right) + 3ft \exp\left(-\frac{t}{RC}\right) - [1 - 3f]RC - 3f\tau \exp\left(-\frac{t}{RC}\right) - [1 - 3f]RC \exp\left(-\frac{2t}{RC}\right) \right] + \frac{C\Delta V \Delta V_{att}}{\tau} \left[\exp\left(-\frac{t}{RC}\right) - 1 \right]. \quad (A.7)$$

Discharging, period 4 ($\tau > 0$):

$$\frac{dq_{dis,4}(t)}{dt} = -C(\Delta V)^2 \frac{RC}{\tau^2} [1 - 3f] \left[1 - \exp\left(-\frac{\tau}{RC}\right) \right]^2 \left[\exp\left(-2\frac{t-\tau}{RC}\right) \right] - \frac{C\Delta V \Delta V_{att}}{\tau} \left[1 - \exp\left(-\frac{\tau}{RC}\right) \right] \left[\exp\left(-\frac{t-\tau}{RC}\right) \right]. \quad (A.8)$$

Discharging ($\tau = 0$):

$$\lim_{\tau \rightarrow 0} \frac{dq_{dis,4}(t)}{dt} = -\frac{(\Delta V)^2}{R} [1 - 3f] \exp\left(-\frac{2t}{RC}\right) - \frac{\Delta V \Delta V_{att}}{R} \exp\left(-\frac{t}{RC}\right). \quad (A.9)$$

A.3. Integral heat

Total charging heat ($\tau > 0$):

$$q_{ch} = -C(\Delta V)^2 \left[\frac{3}{2}f + \frac{RC}{\tau} + \frac{R^2C^2}{\tau^2} \left(\exp\left(-\frac{\tau}{RC}\right) - 1 \right) \right] + C\Delta V \Delta V_{att}. \quad (A.10)$$

Total charging heat ($\tau = 0$):

$$q_{ch} = -\frac{C(\Delta V)^2}{2} [1 + 3f] + C\Delta V \Delta V_{att}. \quad (A.11)$$

Total discharging heat ($\tau > 0$):

$$q_{dis} = -C(\Delta V)^2 \left[-\frac{3}{2}f + \left(\frac{RC}{\tau} \right)^2 \exp\left(-\frac{\tau}{RC}\right) + \frac{RC}{\tau} - \frac{(RC)^2}{\tau^2} \right] - C\Delta V \Delta V_{att}. \quad (A.12)$$

Total discharging heat ($\tau = 0$):

$$q_{dis} = -\frac{C(\Delta V)^2}{2} [1 - 3f] - C\Delta V \Delta V_{att}. \quad (A.13)$$

Total reversible heat for charging (opposite for discharging):

$$q_{rev} = -\frac{3}{2}fC(\Delta V)^2 + C\Delta V \Delta V_{att}. \quad (A.14)$$

Total Joule heat ($\tau > 0$, same for charging and discharging):

$$q_{irr} = -C(\Delta V)^2 \left[\frac{RC}{\tau} + \frac{R^2C^2}{\tau^2} \left(\exp\left(-\frac{\tau}{RC}\right) - 1 \right) \right]. \quad (A.15)$$

Total Joule heat ($\tau = 0$, same for charging and discharging):

$$q_{irr} = -C(\Delta V)^2. \quad (A.16)$$

Appendix B. Supplementary material

Supplementary material related to this article can be found online at <https://doi.org/10.1016/j.electacta.2023.141957>.

Derivations of the formulas that are given in the Appendix A, and additional figures, of the same type as Figs. 3, 4, and 6 for charging potentials ΔV of +0.3 V, -0.3 V, and -0.5 V.

References

- [1] M. Guo, G. Sikha, R. White, Single-particle model for a lithium-ion cell: Thermal behavior, *J. Electrochem. Soc.* 158 (2011) A122–A132.
- [2] L. Song, Z. Xiao, Y. Zhou, Thermo-electrochemical study on LiMn_2O_4 lithium-ion cells during charge-discharge process, *Electrochim. Acta* 114 (2013) 611–616.
- [3] J. Schiffer, D. Linzen, D.U. Sauer, Heat generation in double layer capacitors, *J. Power Sources* 160 (2006) 765–772.
- [4] X. Zhang, W. Wang, J. Lu, L. Hua, J. Heng, Reversible heat of electric double-layer capacitors during galvanostatic charging and discharging cycles, *Thermochim. Acta* 636 (2016) 1–10, <http://dx.doi.org/10.1016/j.tca.2016.04.014>.
- [5] Q. Wang, B. Jiang, Q.F. Xue, H.L. Sun, B. Li, H.M. Zou, Y.Y. Yan, Experimental investigation on EV battery cooling and heating by heat pipes, *Appl. Therm. Eng.* 88 (2015) 54–60.
- [6] Z.G. Qu, Z.Y. Jiang, Q. Wang, Experimental study on pulse self-heating of lithium-ion battery at low temperature, *Int. J. Heat Mass Transfer* 135 (2019) 696–705.
- [7] B.C. Chen, C.Y. Ho, Y.H. Tsai, Y.C. Lee, M.Y. Wen, Analysis of electrical heating in hollow carbon nanoparticles as supercapacitor electrodes for lithium batteries, *J. Nanosci. Nanotechnol.* 16 (2016) 9278–9283.
- [8] M. Al Sakka, H. Gualous, J. van Mierlo, H. Culcu, Thermal modeling and heat management of supercapacitor modules for vehicle applications, *J. Power Sources* 194 (2009) 581–587.
- [9] L.H.J. Rajmakers, D.L. Danilov, R.A. Eichel, P.H.L. Notten, A review on various temperature-indication methods for Li-ion batteries, *Appl. Energy* 240 (2019) 918–945.
- [10] M. Chen, D. Ouyang, S. Cao, J. Liu, Z. Wang, J. Wang, Effects of heat treatment and SOC on fire behaviors of lithium-ion batteries pack, *J. Therm. Anal. Calorim.* 136 (2018) 2429–2437, <http://dx.doi.org/10.1007/s10973-018-7864-9>.
- [11] Y. Dandeville, P. Guillemet, Y. Scudeller, O. Crosnier, L. Athouel, T. Brousse, Measuring time-dependent heat profiles of aqueous electrochemical capacitors under cycling, *Thermochim. Acta* 526 (2011) 1–8.
- [12] Z. Cheng, X. Ji, D.G. Cahill, Battery absorbs heat during charging uncovered by ultra-sensitive thermometry, *J. Power Sources* 518 (2022) 230762.
- [13] J.M. Sherfey, A. Brenner, Electrochemical calorimetry, *J. Electrochem. Soc.* 105 (1958) 665–672.
- [14] J. Marcicki, X. Yang, Model-based estimation of reversible heat generation in lithium-ion cells, *J. Electrochem. Soc.* 161 (2014) A1794–A1800.
- [15] K.E. Thomas, J. Newman, Heats of mixing and of entropy in porous insertion electrodes, *J. Power Sources* 119–121 (2003) 844–849.
- [16] R.J. Noll, J.M. Hughes, Heat evolution and electrical work of batteries as a function of discharge rate: Spontaneous and reversible processes and maximum work, *J. Chem. Educ.* 95 (2018) 852–857.
- [17] A. Gunnarshaug, P. Vie, S. Kjelstrup, Review—Reversible heat effects in cells relevant for lithium-ion batteries, *J. Electrochem. Soc.* 168 (2021) 050522.
- [18] S. Porada, R. Zhao, A. van der Wal, V. Presser, P.M. Biesheuvel, Review on the science and technology of water desalination by capacitive deionization, *Prog. Mater. Sci.* 58 (2013) 1388–1442.
- [19] M.E. Suss, S. Porada, X. Sun, P.M. Biesheuvel, J. Yoon, V. Presser, Water desalination via capacitive deionization: What is it and what can we expect from it? *Energy Environ. Sci.* 8 (2015) 2296–2319.
- [20] L. Wang, Y. Zhang, K. Moh, V. Presser, From capacitive deionization to desalination batteries and desalination fuel cells, *Curr. Opin. Electrochem.* 29 (2021) 100758.
- [21] P. Simon, Y. Gogotsi, Perspectives for electrochemical capacitors and related devices, *Nature Mater.* 19 (2020) 1151–1163.
- [22] Y. Wang, Y. Song, Y. Xia, Electrochemical capacitors: Mechanism, materials, systems, characterization and applications, *Chem. Soc. Rev.* 45 (2016) 5925–5950, <http://dx.doi.org/10.1039/C5CS00580A>.
- [23] A.C. Forse, C. Merlet, J.M. Griffin, C.P. Grey, New perspectives on the charging mechanisms of supercapacitors, *J. Am. Chem. Soc.* 138 (2016) 5731–5744.
- [24] S. Porada, L. Weinstein, R. Dash, A. van der Wal, M. Bryjak, Y. Gogotsi, P.M. Biesheuvel, Water desalination using capacitive deionization with microporous carbon electrodes, *ACS Appl. Mater. Interfaces* 4 (2012) 1194–1199.
- [25] S. Porada, L. Borchardt, M. Oschatz, M. Bryjak, J.S. Atchison, K.J. Keesman, S. Kaskel, P.M. Biesheuvel, V. Presser, Direct prediction of the desalination performance of porous carbon electrodes for capacitive deionization, *Energy Environ. Sci.* 6 (2013) 3700–3712.
- [26] C. Lian, M. Janssen, H. Liu, R. van Roij, Blessing and curse: How a supercapacitor's large capacitance causes its slow charging, *Phys. Rev. Lett.* 124 (2020) 076001, <http://dx.doi.org/10.1103/PhysRevLett.124.076001>.
- [27] M. Janssen, E. Griffioen, P.M. Biesheuvel, R. van Roij, B. Ern , Coulometry and calorimetry of electric double layer formation in porous electrodes, *Phys. Rev. Lett.* 119 (2017) 166002.
- [28] O. Munteshari, J. Lau, A. Krishnan, B. Dunn, L. Pilon, Isothermal calorimeter for measurements of time-dependent heat generation rate in individual supercapacitor electrodes, *J. Power Sources* 374 (2018) 257–268.

- [29] A.L. d'Entremont, L. Pilon, First-principles thermal modeling of electric double layer capacitors under constant-current cycling, *J. Power Sources* 246 (2014) 887–898.
- [30] A.L. d'Entremont, L. Pilon, Thermal effects of asymmetric electrolytes in electric double layer capacitors, *J. Power Sources* 273 (2015) 196–209.
- [31] A.L. d'Entremont, L. Pilon, First-order thermal model of commercial EDLCs, *Appl. Therm. Eng.* 67 (2014) 439–446.
- [32] M. Janssen, R. van Roij, Reversible heating in electric double layer capacitors, *Phys. Rev. Lett.* 118 (2017) 096001.
- [33] M. Janssen, A. H rtel, R. van Roij, Boosting capacitive blue-energy and desalination devices with waste heat, *Phys. Rev. Lett.* 113 (2014) 268501.
- [34] S. Porada, H.V.M. Hamelers, P.M. Biesheuvel, Electrostatic cooling at electrolyte-electrolyte junctions, *Phys. Rev. Res.* 1 (2019) 033195.
- [35] F. Glatzel, M. Janssen, A. H rtel, Reversible heat production during electric double layer buildup depends sensitively on the electrolyte and its reservoir, *J. Chem. Phys.* 154 (2021) 064901.
- [36] P. Pelagejcev, F. Glatzel, A. H rtel, Extension of the primitive model by hydration shells and its impact on the reversible heat production during the buildup of the electric double layer, *J. Chem. Phys.* 156 (2022) 034901.
- [37] J.E. Vos, D. Inder Maur, H.P. Rodenburg, L. van den Hoven, S.E. Schoemaker, P.E. de Jongh, B.H. Ern , Electric potential of ions in electrode micropores deduced from calorimetry, *Phys. Rev. Lett.* 129 (2022) 186001, <http://dx.doi.org/10.1103/PhysRevLett.129.186001>.
- [38] J.E. Vos, H.P. Rodenburg, D. Inder Maur, T.J.W. Bakker, H. Siekman, B.H. Ern , Three-electrode cell calorimeter for electrical double layer capacitors, *Rev. Sci. Instrum.* 93 (2022) 124102.
- [39] P.M. Biesheuvel, S. Porada, M. Levi, M.Z. Bazant, Attractive forces in micro-porous carbon electrodes for capacitive deionization, *J. Solid State Electr.* 18 (2014) 1365–1376.
- [40] F.A. Posey, T. Morozumi, Theory of potentiostatic and galvanostatic charging of the double layer in porous electrodes, *J. Electrochem. Soc.* 113 (1966) 176–184.
- [41] G.J. Lee, S.I. Pyun, Theoretical approach to ion penetration into pores with pore fractal characteristics during double-layer charging/discharging on a porous carbon electrode, *Langmuir* 22 (2006) 10659–10665.
- [42] L.E. Helseth, Modelling supercapacitors using a dynamic equivalent circuit with a distribution of relaxation times, *J. Energy Storage* 25 (2019) 100912.
- [43] L.E. Helseth, The self-discharging of supercapacitors interpreted in terms of a distribution of rate constants, *J. Energy Storage* 34 (2021) 102199.
- [44] R. Tivony, S. Safran, P. Pincus, G. Silbert, J. Klein, Charging dynamics of an individual nanopore, *Nat. Comm.* 9 (2018) 4203.
- [45] J. Chmiola, G. Yushin, Y. Gogotsi, C. Portet, P. Simon, P.L. Taberna, Anomalous increase in carbon capacitance at pore sizes less than 1 nanometer, *Science* 313 (2006) 1760–1763.
- [46] J. Chmiola, G. Yushin, R. Dash, Y. Gogotsi, Effect of pore size and surface area of carbide derived carbons on specific capacitance, *J. Power Sources* 158 (2006) 765–772.
- [47] P. Iamprasertkun, W. Hirunpinyopas, A. Keerthi, B. Wang, B. Radha, M.A. Bissett, R.A.W. Dryfe, Capacitance of basal plane and edge-oriented highly ordered pyrolytic graphite: Specific ion effects, *J. Phys. Chem. Lett.* 10 (2019) 617–623.
- [48] Y. Zou, A.S. Walton, I.A. Kinloch, R.A.W. Dryfe, Investigation of the differential capacitance of highly ordered pyrolytic graphite as a model material of graphene, *Langmuir* 32 (2016) 11448–11455.
- [49] L. Fumagalli, A. Esfandiar, R. Fabregas, S. Hu, P. Ares, A. Janardanan, Q. Yang, B. Radha, T. Taniguchi, K. Watanabe, G. Gomila, K.S. Novoselov, A.K. Geim, Anomalous low dielectric constant of confined water, *Science* 360 (2018) 1339–1342.